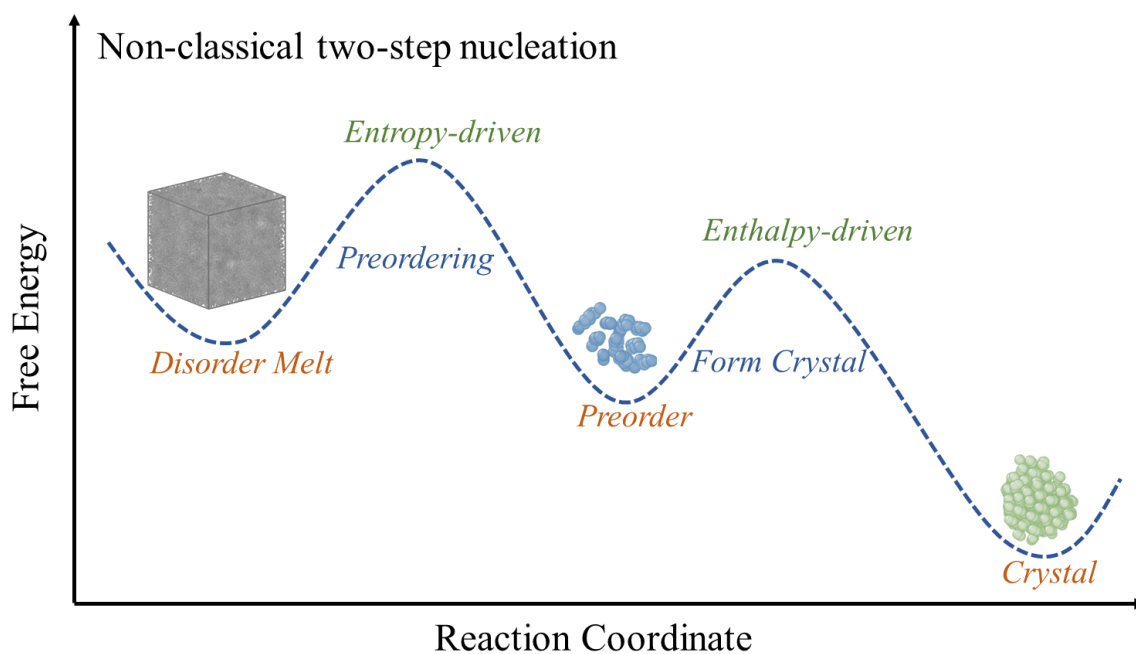


Entropy-Driven Preordering Assists Nucleation in Polyethylene

Renkuan Cao, Fan Peng, Yunhan Zhang, Hao Sun, Ziwei Liu, Tingyu Xu^{*}, and Liangbin Li^{*}

National Synchrotron Radiation Laboratory, Anhui Provincial Engineering Laboratory of Advanced Functional Polymer Film, CAS Key Laboratory of Soft Matter Chemistry, University of Science and Technology of China, Hefei 230026, China

For Table of Contents use only



Corresponding authors, E-mail: tyxu@ustc.edu.cn (T. Y. Xu); lbli@ustc.edu.cn (L. B. Li)

Abstract

Non-classical two-step nucleation including preordering and crystal nucleation has been widely proposed to challenge the one-step nucleation framework in diverse materials, while what drives preordering has not been explicitly resolved yet. With molecular dynamics simulation, we find that two-step nucleation occurs in polyethylene, during which preordering precedes through the coupling between intrachain conformation and interchain orientation orders. Unexpectedly, preordering is driven by entropy rather than enthalpy, during which the interchain translational entropy gain compensates for the intrachain conformation entropy loss. This entropy-driven mechanism resolves the longstanding puzzle why flexible polymers with high entropy penalty still show high nucleation rate and opens a new perspective for understanding nucleation of synthetic and bio-polymers with conformation and orientation orders.

Crystallization is the most important first-order phase transition playing a crucial role in material processing, protein characterization, and pharmaceutical production.^{1, 2} Hence, understanding the formation mechanism of crystals has always been attracting intense interest.^{3, 4} According to the second law of thermodynamics, crystallization can be driven either by enthalpy^{3, 5} or entropy.⁶⁻⁸ In most material systems, the enthalpy gain caused by structural ordering is the main driving force of crystallization,^{3, 9, 10} while for some special systems like colloid crystallization can be driven by entropy gain.^{6, 8}

Either enthalpy- or entropy-driven crystallization mechanism is generally considered under the framework of classical one-step crystallization, while non-classical two-step crystallization has been observed in diverse systems such as colloid, mineral, polymer, protein and etc. with modern experimental¹¹⁻¹⁵ and simulation¹⁶⁻²² techniques. The two-step crystallization models assume that preorder clusters with dense or structure-order form prior to the emergence of crystal, while crystal nuclei appear inside these clusters by structural ordering.⁴ Compared to the one-step crystallization, preorder in two-step crystallization reduces the nucleation barrier and consequently accelerates crystallization,⁴ as illustrated in Figure 1. Here enthalpy and entropy may play different roles in preordering and crystal nucleation, which, however, have not been clarified yet.

Due to the unique chain flexibility, polymer crystallization has to overcome large conformation entropy penalty caused by chain straightening, which is commonly regarded as an enthalpy-driven process.^{23, 24} A longstanding puzzle in polymer community is why flexible polymers like polyethylene (PE) with large conformation entropy penalty still nucleate so fast that fully amorphous structure has never obtained by quenching. This puzzle may be answered by two-step nucleation. In preordering flexible chain transforms

into straight segments through conformational ordering,²⁵ during which the enthalpy gain is weak while the conformational entropy loss ΔS_c is high. This implies that enthalpy gain is not the main driving force in preordering and an unrevealed driving force is required to balance conformational entropy loss ΔS_c . Akin to liquid crystals, the orientation and conformational orders have been confirmed to occur before the onset of polymer crystallization.^{18, 26-30} If the orientation order contributes a translational entropy gain ΔS_{tr} to serve as the hidden driving force in the preordering, contrary to common sense the largest barrier ΔS_c in polymer crystallization would not be overcome by enthalpy, but instead by entropy.

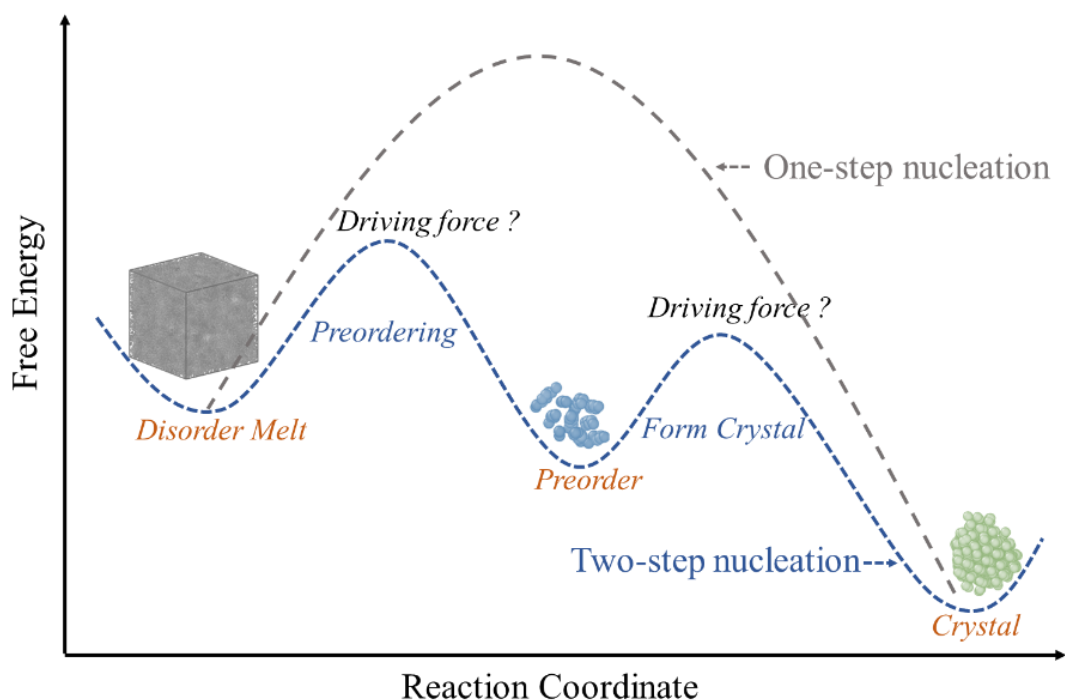


Figure 1. Schematic illustration of the free energy landscape for one-step versus two-step crystallization.

To unveil the respective roles of enthalpy and entropy in the preordering process of polymer crystallization, we employ molecular dynamics (MD) simulation to study the early stage of PE crystallization. Preorders with coupled intrachain conformation and interchain orientation orders are observed prior to crystallization, which is demonstrated to be an entropy-driven mechanism arising from excluded volume effects.

We utilize a united atom force field initially proposed by Paul, Yoon, and Smith,³¹ and subsequently refined by Waheed (see Supporting Information).³² All simulations are performed in the *NPT* ensemble, with the pressure maintained at 1 *atmosphere*. The pressure and temperature are controlled by the Nosé-Hoover barostat and thermostat, employing damping parameters of 5 *ps* and 0.5 *ps*. A time step of 5 *fs* is utilized throughout the simulations. Our system contains 250 C400 chains and follows the procedure illustrated in Figure 2A. The initial configuration undergoes an isothermal relaxation simulation at 600 *K* for 60 *ns* to achieve the equilibrium melt, see Supporting Information. Subsequently, the equilibrium melt is quenched to 300 *K* at a cooling rate of 60 *K/ns*, followed by an 800 *ns* isothermal simulation. The melting temperature is measured at 418.5 *K*, the undercooling is 28.3%, see Supporting Information.

By employing MD simulation, we study the early stage of PE quiescent crystallization (see Figure 2A), during which, the evolution of crystallinity (Φ_c) and the average enthalpy change per particle (Δh) as a function of time are measured, see Figure 2B. Crystalline regions are identified using the cylindrical order parameter ($u_6 > 0.15$ and $u_8 > 0.15$), as proposed in our previous work.¹⁹ The simulation system undergoes a re-equilibration of enthalpy in the first ~ 100 *ns* after quenching and an induction period of about 460 *ns* before the onset of crystallization, they are denoted as early stages. It is seen that Δh almost

presents a platform in the induction period. Crystallization begins at $t > 560$ ns, Δh decreases gradually and the rate accelerates as the crystallization proceeds.

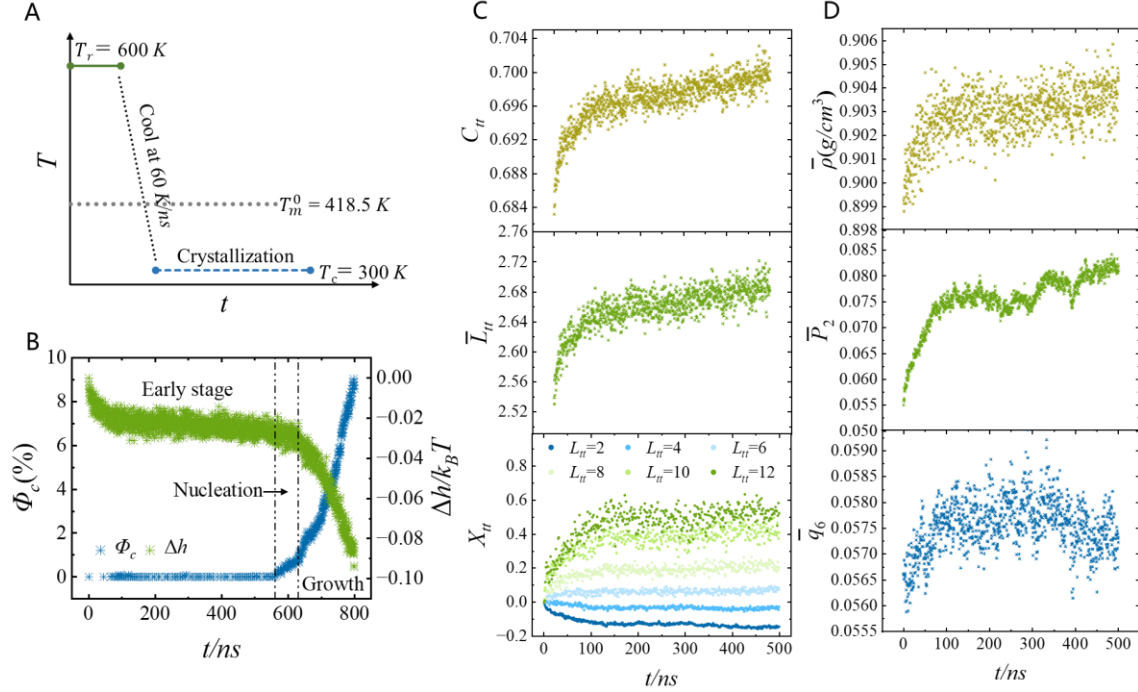


Figure 2. (A) Time-temperature protocols of the simulation procedure. (B) The crystallinity (Φ_c) and the average enthalpy change per particle (Δh) versus time during isothermal crystallization. (C) The time evolution of intra-chain order including the *trans* fraction (C_{tt}), the average length of continuous *trans-trans* segments (L_{tt}), and the rate of increase of *trans* segments, defined as $X_{tt} = [N_{L_{tt}}(t) - N_{L_{tt}}(0)]/N_{L_{tt}}(0)$. (D) The time evolution of three types of inter-chain order including average local density (ρ), local orientation (P_2), and bond orientation order parameter (q_6).

The temporal variations of intra- and inter-chain order parameters in the induction period are illustrated in Figure 2C and 2D. It is characterized by the *trans* fraction (C_{tt}), the average length of continuous *trans-trans* segments (\bar{L}_{tt}), and the rate of increase of *trans* segments,

defined as $X_{tt} = [N_{L_{tt}}(t) - N_{L_{tt}}(0)] / N_{L_{tt}}(0)$. Here, *gauche* and *trans* are defined as the conformation which dihedral angle $|\varphi| < 120^\circ$ and $|\varphi| > 120^\circ$, see Supporting Information. $N_{L_{tt}}(t)$ and $N_{L_{tt}}(0)$ denote the number of L_{tt} segments at t ns and 0 ns, respectively. As depicted in Figure 2C, both the C_{tt} and \bar{L}_{tt} initially increase steeply in the first 100 ns and then slowly over time. For short *trans* segments with $L_{tt} \leq 4$, X_{tt} decreases with time. Conversely, for long *trans* segments with $L_{tt} > 4$, X_{tt} increases with time. This indicates that the intra-chain conformational order (*gauche*-to-*trans* transition) occurs prior to the formation of the crystal. The time evolutions of three inter-chain order parameters, namely, average local density ($\bar{\rho}$), local orientation (\bar{P}_2), and bond orientation order parameter (\bar{q}_6) are systematically measured (see Figure 2D). These parameters are ensemble-averaged for each system snapshot (detailed calculation methods are elaborated in the Supporting Information). Similar to intra-chain parameters C_{tt} and \bar{L}_{tt} , the inter-chain parameters $\bar{\rho}$, and \bar{P}_2 also exhibit rapid and gradual two-stage increases, while \bar{q}_6 follows a rapid increase and gradual decrease trend over time. These observations suggest that the inter-chain order, characterized by $\bar{\rho}$, \bar{P}_2 , and \bar{q}_6 , precedes the formation of the crystal. This observation is consistent with findings from previous experiments³⁰ and simulation results.^{18, 27}

To verify the coupling between intra- and inter-chain order, contour maps of ρ , P_2 , and q_6 in t - L_{tt} space are plotted in Figure 3A. As L_{tt} increases, ρ , P_2 , and q_6 increase. Regions with higher L_{tt} values correspond to higher values of ρ , P_2 , and q_6 , indicating a coupling between L_{tt} and these inter-chain order parameters. To find the correlation relationship, we measure the Pearson correlation coefficient ($C(L_{tt}, O)$) of L_{tt} and O as a function of time t , where O represents the ρ , P_2 , and q_6 . The $C(L_{tt}, O)$ is calculated by

$$C(L_{tt}, O) = \frac{\sigma[L_{tt}(t), O(t)]}{\sigma[L_{tt}(t)] \sigma[O(t)]} \quad (1)$$

where $\sigma[x, y]$ denotes the covariance between x and y , and $\sigma[x]$ denotes the square root of variance of x . As shown in Figure 3B, $C(L_{tt}, P_2)$ increases over time and is consistently much larger than $C(L_{tt}, \rho)$ and $C(L_{tt}, q_6)$. It indicates that the coupling of conformation and density considered by Olmsted *et al.*³³ is extremely weak and insufficient to trigger spinodal decomposition. The predominant coupling mode between intra- and inter-chain order is the interplay of conformation and orientation. By this predominant coupling mode, preorders with coupled intra-chain conformation and inter-chain orientation orders appear prior to the emergence of crystal and assist the subsequent crystallization, see Figure 3C.

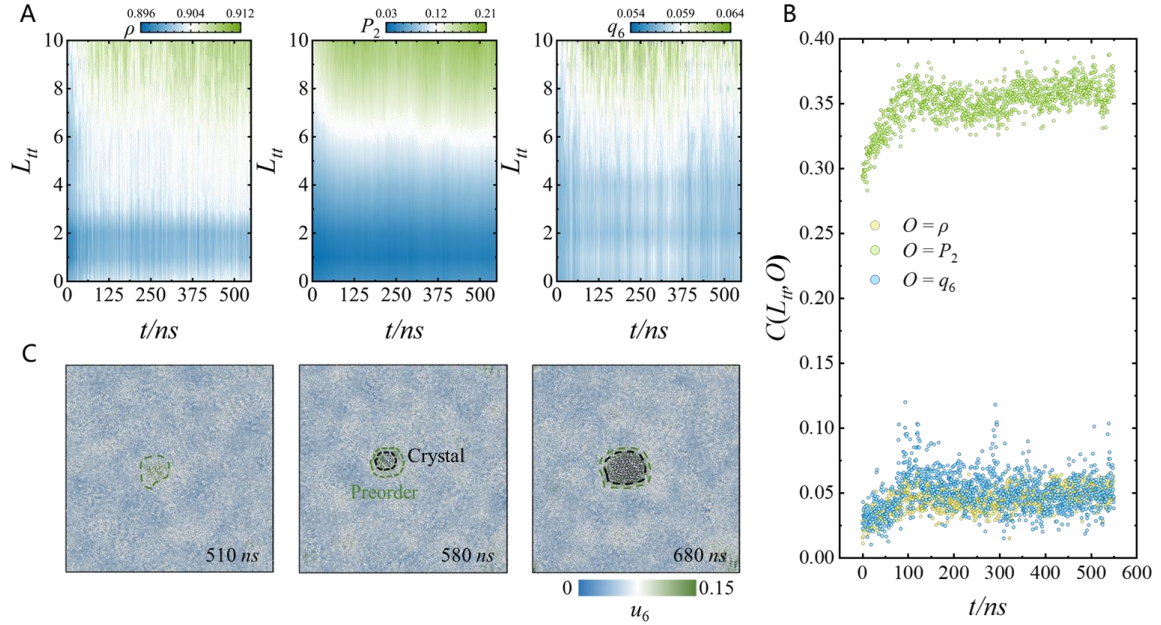


Figure 3. (A) The contour map of the length of continuous *trans-trans* segments L_{tt} for crystallization time and inter-chain order parameters, including local density (ρ), local orientation (P_2), and bond orientation order parameters (q_6). (B) The Pearson correlation

coefficient ($C(L_{it}, O)$) of L_{it} and O as a function of time, where, O represents the ρ , P_2 , and q_6 . (C) System snapshot at 510 ns, 580 ns, and 680 ns. The amorphous particles and crystal particles are rendered with u_6 and black.

The enthalpy change in preordering is weak as shown in Figure 2B, suggesting an unrevealed driving force may exist. The *gauche-trans* transition involves a competition between the potential energy gain Δh and the entropy loss Δs per particle, which can be described by the free energy gap per particle $\Delta f = \Delta h - T\Delta s$. Δf can be determined by counting the number distribution of *trans-trans* segments at different simulation times.³⁴ For a given time, the distribution of *trans-trans* segment numbers of different L_{it} follows the Boltzmann distribution, suggesting that their number is governed by energy. Thus, the formula $N_{L_{it}} = N_0 \exp(-\Delta E/k_B T)$ is derived,³⁴ where k_B is the Boltzmann constant and N_0 is a constant. By taking the natural logarithm, it can be transformed to

$$\ln N_{L_{it}} = \ln N_0 + \left(-\frac{\Delta E}{k_B T}\right) \quad (2)$$

In Figure 4A, the plot of $\ln N_{L_{it}}$ versus L_{it} at 300 ns shows a linear relationship (more data are plotted in the Supporting Information), leading to the assumption that ΔE is equal to $L_{it} \Delta f$. Therefore, Eq. (2) can be rewritten as

$$\ln N_{L_{it}} = \ln N_0 + \left(-\frac{L_{it} \Delta f}{k_B T}\right) \quad (3)$$

Δf can be obtained from the slope of linear fit in Figure 4A. This linearity across all simulation times indicates that Δf remains constant versus L_{it} . Figure 4B depicts the variation of Δf over simulation time (black circles). To facilitate the comparison, Δf at 0 ns is selected as the reference zero free energy. It is seen that Δf decreases with time,

suggesting that inter-chain coupling interaction (orientation) reduces Δf and facilitates the *gauche-trans* transition.

Δf can be divided into the intra-chain free energy (Δf_{intra}) along the chain direction and inter-chain coupling free energy (Δf_{inter}) deviating from the chain direction,

$$\Delta f = \Delta f_{intra} + \Delta f_{inter} = \Delta E_{intra} - T \Delta s_c + \Delta E_{inter} - T \Delta s_o \quad (4)$$

ΔE_{intra} is the intra-chain energy difference between the *gauche* and *trans* state, which represents the change of intra-chain potential energy. It includes the energy gained from bond stretching, bond angle bending, and dihedral angle rotation. Until 550 ns, ΔE_{intra} has decreased by about 0.0122 $k_B T$, as shown in Figure 4B (blue circle). The change in intra-chain entropy is predominantly contributed by conformation entropy change Δs_c . In the present work, we quantify conformational entropy using dihedral angle entropy, as described in references.³⁵⁻³⁷ It is written as

$$s_c = -k_B (\sum_{i=1}^{N_g} p_i \ln p_i + \ln N_g) \quad (5)$$

where p_i represents the probability of a dihedral angle occurring within the i th grid, with N_g being the number of equally divided isometric grids spanning the entire range of dihedral angles. The variation of dihedral angle entropy (Δs_c) is insensitive to the value of N_g , as detailed in the Supporting Information. As depicted in Figure 4B (green circle), over the period up to 550 ns, $-T \Delta s_c$ increases by approximately 0.0235 $k_B T$. The *gauche-trans* transition increases chain rigidity, reducing freedom along the chain direction and thereby imposing an entropy penalty that hinders the formation of *trans* configurations. The change in the intra-chain free energy, $\Delta f_{intra} = \Delta E_{intra} - T \Delta s_c$, becomes positive over time, thereby inhibiting the *gauche-trans* transition. Evidently, the decrease in Δf is driven by the change

in inter-chain coupling free energy, $\Delta f_{inter} = \Delta E_{inter} - T \Delta s_o$. ΔE_{inter} represents the change in inter-chain potential energy (non-bond interaction energy) gain. As shown in Figure 4B (blue triangle), over the period up to 550 ns, ΔE_{inter} decreases by about 0.0034 $k_B T$, as illustrated by the green diamond. This reduction is significantly smaller compared to the decrease in Δf . From these findings, it is inferred that the decrease in Δf is predominantly influenced by the change in coupling entropy $-T \Delta s_o$, which is calculated with Eq. (4), as depicted in Figure 4B (blue triangle). Therefore, this observation leads to the conclusion that the preorder coupling mechanism between conformation and orientation is entropy-driven.

Referring to Onsager's lyotropic liquid crystal theory,³⁸ we attribute the coupling entropy Δs_o to the translational entropy Δs_{tr} , which arises from excluding the volume effects. The polymer chain is regarded as a freely-jointed chain composed of the Kuhn segment with length L and diameter D , Δs_{tr} can be written as³⁸⁻⁴⁰

$$\Delta s_{tr} = \frac{1}{2} k_B \rho_{mol} \int d\mathbf{w} \int d\mathbf{w}' f(\mathbf{w}) f(\mathbf{w}') V_{exc}(\mathbf{w}, \mathbf{w}') \quad (6)$$

where the $\rho_{mol} = N/V$ is the number density of Kuhn segments, with N being the number of Kuhn segments and V the volume of the simulated box, respectively. The function $f(\mathbf{w})$ denotes the orientational distribution function of the Kuhn segment. Due to the unavailability of the exact orientation vector \mathbf{w} for each Kuhn segment, the unit chord vector \mathbf{e} (the vector connecting two adjacent particles within the same chain) is used as a substitute. The selection of the unit chord vector does not significantly alter Δs_{tr} , as detailed in the Supporting Information. The $V_{exc}(\mathbf{w}, \mathbf{w}')$ represents the excluded volume between two Kuhn segments oriented along \mathbf{w} and \mathbf{w}' . It can be expressed as

$$V_{exc}(\mathbf{w}, \mathbf{w}') = 2L^2D|\sin\theta_{\mathbf{w}, \mathbf{w}'}| + 2\pi LD^2 + \frac{4}{3}\pi D^3 \quad (7)$$

where $\theta_{\mathbf{w}, \mathbf{w}'}$ denotes the angle between vectors \mathbf{w} and \mathbf{w}' . The diameter D can be calculated using the second virial coefficient as $B_2 = \frac{2}{3}\pi D^3$ ⁴¹⁻⁴⁴ and expresses as

$$B_2 = -2\pi \int [\exp\left(-\frac{u(r)}{k_B T}\right) - 1] r^2 dr \quad (8)$$

where $u(r)$ is the non-bond interaction term of the force field (see the Supporting Information for more detailed information). The length of Kuhn segment L can be calculated by $L = \frac{C_\infty n l^2}{R_{max}}$, where C_∞ is Flory characteristic ratio and R_{max} is the contour length. Here, $l = 0.153$ nm represents the length and number of each C-C bond, and $n = 399$ is the number of C-C bonds per chain. By combining Eq. (6) to eq. (8), ΔS_{tr} can be quantitatively calculated. Figure 4C illustrates the linear relationship between ΔS_o and ΔS_{tr} with slope of 0.92, indicating that the entropy increases in ΔS_o is mainly contributed by ΔS_{tr} .

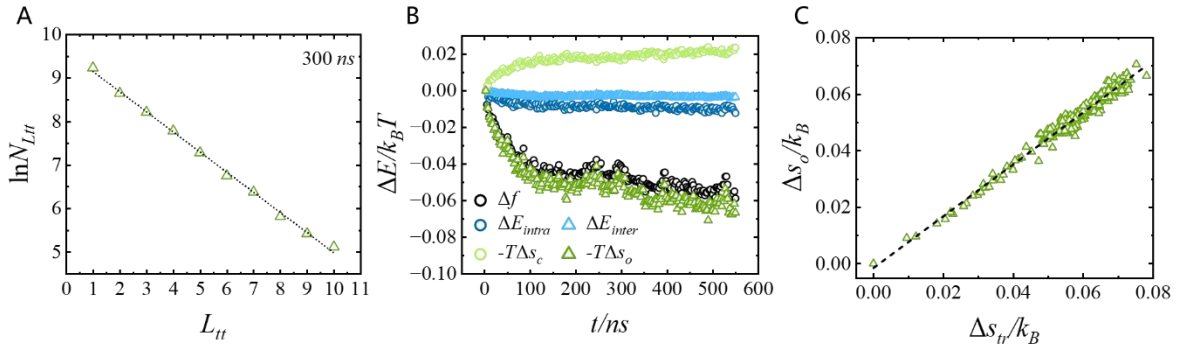


Figure 4. (A) The distribution of $\ln N_{L_{tt}}$ as a function of the length of continuous *trans-trans* segments L_{tt} at 300 ns. The $N_{L_{tt}}$ represents the number of *trans-trans* segments. (B) The evolution of free energy and its components over simulation time. (C) Comparison of translation entropy with coupling entropy.

The existence and the nature of preorders have been widely reported in various material systems. Preorder reduces the nucleation barrier of crystal and accelerates crystallization is emphasized as compared to the classical one-step nucleation (see Figure 1). Whilst how preorder crosses the free energy barrier and what is the main driving force are not explicitly studied yet except in colloid and hard particle systems with designed entropy and enthalpy interactions. Our results reveal that the preordering of polymer precedes via coupling between conformation and orientation order. The translational entropy caused by the excluded volume effect of conformationally ordered rigid segments compensates for intrachain conformational entropy loss and drives preordering. Crystallization of flexible polymer is generally considered to be hard as it has to overcome the large conformation entropy penalty. This entropy-driven mechanism gives an answer to the longstanding puzzle that the crystallization rate of flexible polymers like PE is so fast that a fully amorphous structure has never been obtained. Through coupling between intrachain conformation and interchain orientation orders, the large conformation entropy penalty is compensated by the translational entropy, which results in the formation of preorder and subsequently accelerates the crystallization of flexible polymers. Current entropy-driven mechanism for preordering provides a generic model with two mutually compensating entropies, it may not only exist in synthetic polymers, but also presents in natural macromolecules like protein with similar conformation and orientation orders, for which non-classical two-step crystallization has been largely reported.

In summary, we reveal a two-step crystallization process of disordered melt \rightarrow preorder \rightarrow crystal. The first step is a process of mutual coupling between intrachain conformation

and interchain orientation orders. The translational entropy gain caused by orientation order compensates for the conformation entropy loss. It is crucial, particularly for flexible polymers with weak intra-chain interactions, where a high entropy penalty hinders long *trans-trans* segment formation. For the second step (i.e., precursor \rightarrow crystal), enthalpy gain is significant, indicating that it is enthalpy-driven. Our results reveal that enthalpy and entropy play different roles in these two steps, opening a new perspective to understanding polymer crystallization.

ACKNOWLEDGMENTS

This work is supported by the National Key R&D Program of China (2020YFA0405800) and the National Natural Science Foundation of China (51633009).

REFERENCES

1. De Yoreo, J. J.; Gilbert, P. U. P. A.; Sommerdijk, N. A. J. M.; Penn, R. L.; Whitlam, S.; Joester, D.; Zhang, H.; Rimer, J. D.; Navrotsky, A.; Banfield, J. F.; Wallace, A. F.; Michel, F. M.; Meldrum, F. C.; Cölfen, H.; Dove, P. M., Crystallization by particle attachment in synthetic, biogenic, and geologic environments. *Science* **2015**, *349* (6247).
2. Cui, K.; Ma, Z.; Tian, N.; Su, F.; Liu, D.; Li, L., Multiscale and Multistep Ordering of Flow-Induced Nucleation of Polymers. *Chemical Reviews* **2018**, *118* (4), 1840-1886.
3. Karthika, S.; Radhakrishnan, T. K.; Kalaichelvi, P., A Review of Classical and Nonclassical Nucleation Theories. *Crystal Growth & Design* **2016**, *16* (11), 6663-6681.
4. Li, J.; Deepak, F. L., In Situ Kinetic Observations on Crystal Nucleation and Growth. *Chemical Reviews* **2022**, *122* (23), 16911-16982.
5. Thanh, N. T. K.; Maclean, N.; Mahiddine, S., Mechanisms of Nucleation and Growth of Nanoparticles in Solution. *Chemical Reviews* **2014**, *114* (15), 7610-7630.
6. Manoharan, V. N., Colloidal matter: Packing, geometry, and entropy. *Science* **2015**, *349* (6251).
7. Hu, H.; Ruiz, P. S.; Ni, R., Entropy Stabilizes Floppy Crystals of Mobile DNA-Coated Colloids. *Physical Review Letters* **2018**, *120* (4).
8. Karayiannis, N. C.; Foteinopoulou, K.; Laso, M., Entropy-Driven Crystallization in Dense Systems of Athermal Chain Molecules. *Physical Review Letters* **2009**, *103* (4), 045703.
9. Hoffman, J. D.; Miller, R. L., Kinetic of crystallization from the melt and chain folding in polyethylene fractions revisited: theory and experiment. *Polymer* **1997**, *38* (13), 3151-3212.

10. Strobl, G., Colloquium: Laws controlling crystallization and melting in bulk polymers. *Reviews of Modern Physics* **2009**, *81* (3), 1287-1300.
11. Desgranges, C.; Delhommelle, J., Can Ordered Precursors Promote the Nucleation of Solid Solutions? *Physical Review Letters* **2019**, *123* (19).
12. Savage, J. R.; Dinsmore, A. D., Experimental Evidence for Two-Step Nucleation in Colloidal Crystallization. *Physical Review Letters* **2009**, *102* (19).
13. Tan, P.; Xu, N.; Xu, L., Visualizing kinetic pathways of homogeneous nucleation in colloidal crystallization. *Nature Physics* **2013**, *10* (1), 73-79.
14. Van Driessche, A. E. S.; Ling, W. L.; Schoehn, G.; Sleutel, M., Nucleation of glucose isomerase protein crystals in a nonclassical disguise: The role of crystalline precursors. *Proceedings of the National Academy of Sciences* **2022**, *119* (7).
15. Yamazaki, T.; Kimura, Y.; Vekilov, P. G.; Furukawa, E.; Shirai, M.; Matsumoto, H.; Van Driessche, A. E. S.; Tsukamoto, K., Two types of amorphous protein particles facilitate crystal nucleation. *Proceedings of the National Academy of Sciences* **2017**, *114* (9), 2154-2159.
16. ten Wolde, P. R.; Ruiz-Montero, M. J.; Frenkel, D., Numerical Evidence for bcc Ordering at the Surface of a Critical fcc Nucleus. *Physical Review Letters* **1995**, *75* (14), 2714-2717.
17. Wolde, P. R. t.; Frenkel, D., Enhancement of protein crystal nucleation by critical density fluctuations. *Science* **1997**, *277* 5334, 1975-8.
18. Zhang, W.; Larson, R. G., A metastable nematic precursor accelerates polyethylene oligomer crystallization as determined by atomistic simulations and self-consistent field theory. *The Journal of Chemical Physics* **2019**, *150* (24).
19. Cao, R.; Peng, F.; Nie, C.; Zhang, Y.; Sun, H.; Liu, Z.; Xu, T.; Li, L., Primary Nucleation of Polymer Crystal via Particles Fluctuation with Non-Markovian Effect. *Macromolecules* **2024**, *57* (13), 5979-5990.
20. Sosso, G. C.; Chen, J.; Cox, S. J.; Fitzner, M.; Pedevilla, P.; Zen, A.; Michaelides, A., Crystal Nucleation in Liquids: Open Questions and Future Challenges in Molecular Dynamics Simulations. *Chemical Reviews* **2016**, *116* (12), 7078-7116.
21. Sun, Y.; Zhang, F.; Mendeleev, M. I.; Wentzcovitch, R. M.; Ho, K.-M., Two-step nucleation of the Earth's inner core. *Proceedings of the National Academy of Sciences* **2022**, *119* (2).
22. Kawasaki, T.; Tanaka, H., Formation of a crystal nucleus from liquid. *Proceedings of the National Academy of Sciences* **2010**, *107* (32), 14036-14041.
23. Tang, X.; Chen, W.; Li, L., The Tough Journey of Polymer Crystallization: Battling with Chain Flexibility and Connectivity. *Macromolecules* **2019**, *52* (10), 3575-3591.
24. Zhang, M.; Guo, B.-H.; Xu, J., A Review on Polymer Crystallization Theories. *Crystals* **2016**, *7* (1).
25. Yi, P.; Locker, C. R.; Rutledge, G. C., Molecular Dynamics Simulation of Homogeneous Crystal Nucleation in Polyethylene. *Macromolecules* **2013**, *46* (11), 4723-4733.
26. Nie, C.; Peng, F.; Xu, T.; Ding, Y.; Sheng, J.; Chen, W.; Li, L., Biaxial Stretch-Induced Crystallization of Polymers: A Molecular Dynamics Simulation Study. *Macromolecules* **2021**, *54* (21), 9794-9803.
27. Anwar, M.; Turci, F.; Schilling, T., Crystallization mechanism in melts of short n-alkane chains. *The Journal of Chemical Physics* **2013**, *139* (21).
28. Migler, K. B.; Kotula, A. P.; Hight Walker, A. R., Trans-Rich Structures in Early Stage Crystallization of Polyethylene. *Macromolecules* **2015**, *48* (13), 4555-4561.
29. Chen, X.; Meng, L.; Zhang, W.; Ye, K.; Xie, C.; Wang, D.; Chen, W.; Nan, M.; Wang, S.; Li, L., Frustrating Strain-Induced Crystallization of Natural Rubber with Biaxial Stretch. *ACS Applied Materials & Interfaces* **2019**, *11* (50), 47535-47544.
30. Su, F.; Ji, Y.; Meng, L.; Wang, Z.; Qi, Z.; Chang, J.; Ju, J.; Li, L., Coupling of Multiscale Orderings during Flow-Induced Crystallization of Isotactic Polypropylene. *Macromolecules* **2017**,

50 (5), 1991-1997.

31. Paul, W.; Yoon, D. Y.; Smith, G. D., An optimized united atom model for simulations of polymethylene melts. *The Journal of Chemical Physics* **1995**, *103* (4), 1702-1709.
32. Waheed, N.; Ko, M. J.; Rutledge, G. C., Molecular simulation of crystal growth in long alkanes. *Polymer* **2005**, *46* (20), 8689-8702.
33. Olmsted, P. D.; Poon, W. C. K.; McLeish, T. C. B.; Terrill, N. J.; Ryan, A. J., Spinodal-Assisted Crystallization in Polymer Melts. *Physical Review Letters* **1998**, *81* (2), 373-376.
34. Xie, C.; Tang, X.; Yang, J.; Xu, T.; Tian, F.; Li, L., Stretch-Induced Coil–Helix Transition in Isotactic Polypropylene: A Molecular Dynamics Simulation. *Macromolecules* **2018**, *51* (11), 3994-4002.
35. Ma, R.; Xu, D.; Luo, C.-F., Effect of Crystallization and Entropy Contribution Upon the Mechanical Response of Polymer Nano-fibers: A Steered Molecular Dynamics Study. *Chinese Journal of Polymer Science* **2022**, *41* (3), 465-474.
36. Sultanov, V. I.; Atrazhev, V. V.; Dmitriev, D. V.; Erikhman, N. S.; Furrer, D. U.; Burlatsky, S. F., Microscopic Mechanism of the Large Electrocaloric Effect in Vinylidene Difluoride-Based Polymers. *Macromolecules* **2021**, *54* (8), 3744-3754.
37. Baruah, A.; Rani, P.; Biswas, P., Conformational Entropy of Intrinsically Disordered Proteins from Amino Acid Triads. *Scientific Reports* **2015**, *5* (1).
38. Onsager, L., THE EFFECTS OF SHAPE ON THE INTERACTION OF COLLOIDAL PARTICLES. *Annals of the New York Academy of Sciences* **1949**, *51* (4), 627-659.
39. Binder, K.; Egorov, S. A.; Milchev, A.; Nikoubashman, A., Understanding the properties of liquid-crystalline polymers by computational modeling. *Journal of Physics: Materials* **2020**, *3* (3), 032008.
40. Vroege, G. J.; Lekkerkerker, H. N. W., Phase transitions in lyotropic colloidal and polymer liquid crystals. *Reports on Progress in Physics* **1992**, *55* (8), 1241.
41. Schultz, A. J.; Kofke, D. A., Virial coefficients of model alkanes. *The Journal of Chemical Physics* **2010**, *133* (10).
42. McCoy, J. D.; Mateas, S.; Zorlu, M.; Curro, J. G., The role of excluded volume in polyethylene intermolecular potentials. *The Journal of Chemical Physics* **1995**, *102* (21), 8635-8642.
43. Smith, J. S.; Bedrov, D.; Smith, G. D., A molecular dynamics simulation study of nanoparticle interactions in a model polymer-nanoparticle composite. *Composites Science and Technology* **2003**, *63* (11), 1599-1605.
44. Yu, B.; Liang, H.; Rumyantsev, A. M.; De Pablo, J. J., Isotropic-to-Nematic Transition in Salt-Free Polyelectrolyte Coacervates from Coarse-Grained Simulations. *Macromolecules* **2022**, *55* (21), 9627-9639.